Constraint on the S-wave velocity at the base of the mantle

Eléonore Stutzmann, Lev Vinnik, Ana Ferreira, Satish Singh

▶ **To cite this version:**

Eléonore Stutzmann, Lev Vinnik, Ana Ferreira, Satish Singh. Constraint on the S-wave velocity at the base of the mantle. Geophysical Research Letters, 2000, 27, pp.1571-1574. 10.1029/1999GL010984 . insu-03596941

HAL Id: insu-03596941

https://insu.hal.science/insu-03596941

Submitted on 4 Mar 2022

HAL is a multi-disciplinary open access archive for the deposit and dissemination of scientific research documents, whether they are published or not. The documents may come from teaching and research institutions in France or abroad, or from public or private research centers.

L'archive ouverte pluridisciplinaire **HAL**, est destinée au dépôt et à la diffusion de documents scientifiques de niveau recherche, publiés ou non, émanant des établissements d'enseignement et de recherche français ou étrangers, des laboratoires publics ou privés.

Copyright

GEOPHYSICAL RESEARCH LETTERS, VOL. 27, NO. 11, PAGES 1571-1574, JUNE 1, 2000

Constraint on the S-wave velocity at the base of the mantle

Eléonore Stutzmann[1], Lev Vinnik[2], Ana Ferreira[1], and Satish Singh[1]

Abstract. Some recent seismic studies have suggested the presence of a thin ultra-low P-wave velocity layer (ULVZ) at the base of the mantle, which is interpreted to be due to presence of partial melting. Partial melting would lead to a strong decrease of the S-wave velocity for which there is no seismic evidence. Such a decrease in the S-wave velocity would produce a strong precursor to SKS phase from the conversion of S to P at the upper boundary of the layer. We analyze records of events from the subduction zones in the south-west Pacific region obtained at stations in North America. At the source side, the converted phases propagate in the region, where the ultra-low P-wave velocity has been found earlier. Our analysis demonstrates that either the S-wave velocity drop in this layer is much smaller than predicted by the hypothesis of melting, or the layer is so thin (less than about 10-15 km) that it can not be detected with our technique.

Introduction

Structure of the D" layer at the base of the mantle is of interest, because it may be closely related to the Earth's dynamics. Doornbos and Hilton [1989] suggested that the P-wave velocity in a thin layer at the base of the mantle in the central Pacific is anomalously low. The $SPdKS$ seismic phase generated by earthquakes in subduction zones in the south-west Pacific arrives to North America later than predicted by standard models [Garnero et al. 1993]. $SPdKS$ propagates partly as SKS phase and partly as $Pdiff$ phase along the core-mantle boundary [Kind and Mueller 1975, Choy 1977]. The late arrival of $SPdKS$ phase is explained by a strong reduction of P-wave velocity (-10%) in a layer having variable thickness (5-40km) at the base of the mantle (for a review see Garnero et al., 1998). Strong lateral heterogeneity of the ULVZ is manifested by large differences in amplitudes and travel times of SPdKS phase at nearly identical wave paths [Garnero and Helmberger, 1998]. The low P-wave velocity (-10%) can be caused by partial melt which implies a 3:1 ratio between S-wave and P-wave velocities and thus around 30% of S-wave velocity reduction [Williams and Garnero 1996]. However, compelling evidence of partial melting in D" is missing. The observations related to ULVZ have been made with the P waves, whereas the idea of melting can be tested only with the data sensitive to S-wave velocity. There is a trade-off between the values of P-wave and S-wave velocities, density and thickness of the ultra low velocity layer inferred from the observations of $SPdKS$ phase [Garnero and Helmberger, 1998].

In this study we test the hypothesis of partial melting with a technique, which allows us to take into account the strong lateral heterogeneity of the lowermost mantle and to avoid the trade-off between various parameters of the ULVZ. If a layer of reduced S-wave velocity is present at the base of D", its upper boundary may generate S-to-P converted phase that would arrive as a precursor to SKS phase. S-to-P converted phases are strongly sensitive only to the S-wave velocity contrast at the discontinuity, which practically excludes a trade-off between S-wave velocity and the other parameters of the layer. Moreover, the required sharpness of the

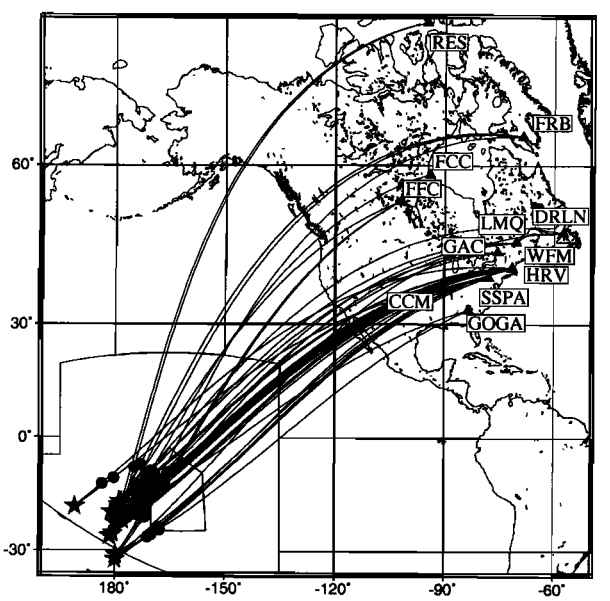

Figure 1. Projections of raypaths of SKS phase between events (stars) and stations (triangles). The points of conversion from S to P on the source side are marked by filled circles. Large and small polygons represent the area of ultra-low velocity according to Garnero et al. [1998] and Garnero and Helmberger [1996].

[1] Dept. Sismologie, IPGP, 4 Place Jussieu, 75232 Paris 05, France.

[2]Institute of physics of the Earth, B. Gruzinskaya 10, 123810 Moscow, Russia

Copyright 2000 by the American Geophysical Union.

Paper number 1999GL010984.
0094-8276/00/1999GL010984$05.00

boundary is not limited by a few kilometers. The data base of our study consists of the broad-band records of intermediate and deep events in the south-west Pacific at digital seismograph stations in North America. Epicenters of these seismic events, seismograph stations, surface projections of the wave paths and points of conversion at CMB are shown in Figure 1. We assume in agreement with previous studies, that the anomalous layer is present only at the source side of the wavepaths. The points of conversion for these paths are located within the area where ULVZ has been previously reported [Garnero et al. 1998].

Modeling the effect of ULVZ

The product of transmission coefficients for SKS at CMB (from the mantle to the core and back) is independent of frequency for the values of ray parameter, p, less than 255 s [Choy 1977]. The critical value of the ray parameter for SKS is achieved at an epicentral distance of around 107°, and the ray theory is applicable at larger distance. In the presence of ULVZ the critical value of p for the S-to-P conversion at CMB is reached at a smaller distance, but for a thin ULVZ the critical distance for its upper boundary remains practically the same. In the overcritical distance range, where the ray theory is applicable, the lateral heterogeneities of D" and in particular the difference between D" at the source and the receiver side can be easily taken into account.

We consider the model shown in Figure 2, in which ULVZ is present only at the source side, whereas at the receiver side the model is IASP91 [Kennett 1991]. The phase which arrives instead of SKS is S^SKS, where first S is for the mantle and D" layer above the ULVZ at the source side, second S is for the path in ULVZ and KS is for the rest of the ray path up to the receiver. The phase, converted from the upper boundary of ULVZ is S^PKS, where P is for the path in ULVZ. For ULVZ with velocity reductions $\delta V_P = -10\%$ and $\delta V_S = -30\%$, the amplitude ratio S^PKS/S^SKS is close to 0.6, and practically independent of distance in the distance range of interest (109 to 122 degrees). For the S and P velocities reduced by 30% and 10%, respectively, the layer thickness of 30, 20 and 10 km yields the lead time of S^PKS around 3.8 s, 2.3 s and 1.3 s. In the epicentral distance range of interest, these values are almost independent of distance.

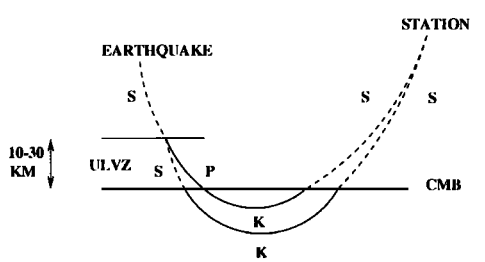

Figure 2. Raypaths of phases S^SKS and S^PKS.

Table 1. List of events.

Date	Lat. Long. Depth	Stations & dist.(°)
86/05/26	-20.24 179.02 568	WFM 118
86/06/16	-21.86 -178.86 565	WFM 117
86/06/28	-19.95 -175.71 222	WFM 114
87/03/19	-20.29 -175.96 215	WFM 114
89/03/11	-17.78 -174.77 244	HRV 111
90/06/08	-18.51 -178.92 504	HRV 115
90/07/22	-23.15 -179.83 559	HRV 119
91/09/30	-20.67 -178.52 590	HRV 116, WFM 116
92/07/11	-22.45 -177.96 394	HRV 117
93/03/21	-17.70 -178.41 608	HRV 114
93/04/16	-17.54 -178.75 592	GAC 112
94/02/11	-18.88 169.08 223	CCM 109, HRV 124
94/03/09	-17.69 -178.11 568	DRLN 123, FRB 114 HRV 114, LMQ 115 WFM 114
94/03/31	-22.04 -179.30 607	FRB 119, GAC 115 HRV 117
94/10/27	-25.75 179.38 541	HRV 121, LMQ 122 FCC 109
95/01/17	-20.70 -179.13 649	SSPA 112
96/08/05	-20.71 -178.16 555	HRV 116, RES 108
96/11/05	-30.95 -179.72 367	FFC 108, GOGA 111
97/05/25	-32.02 -179.94 345	CCM 108, FFC 109 HRV 124, SSPA 119
97/09/04	-26.45 178.52 621	HRV 122, SSPA 117
98/05/16	-22.27 -179.35 609	HRV 118, SSPA 113

Synthetic seismograms were computed using Gaussian beam technique [Weber 1988]. Focal plane solutions and source functions were adopted from Harvard catalog and from the University of Michigan catalog [Ruff and Miller, 1994], respectively. The synthetic seismograms were convolved with attenuation operator. According to Choy and Cormier [1986], Q in most of the mantle is high at frequencies much higher than 0.3 Hz and low at frequencies much lower than 0.3 Hz. Our data have a limited frequency range around 0.3 Hz. Therefore we assumed t^* to be independent of frequency. For different stations the value of t^* varied between 1.5 and 2.5 s in a broad agreement with the estimates by Choy and Cormier [1986]. Our synthetic seismograms look different from those computed with a reflectivity method by Garnero and Helmberger [1998] for comparable models. There are three main reasons for this. First, the ULVZ layer in the models considered by Garnero and Helmberger is present in both the source and the receiver regions, whereas in our models it is present only on the source side. Second, our seismograms have much shorter periods. At shorter periods the precursor is better separated from the main phase. Third, the synthetic seismograms which are calculated with 1-D reflectivity method contain multiple reflections in ULVZ. These phases can propagate within a continuous, laterally homogeneous ULVZ, but the assumption of lateral homogeneity is not applicable to the D" layer beneath the Pacific [Vinnik et al. 1998].

Data analysis

The broad-band seismograms (Table 1) were deconvolved by the instrument response to obtain displace-

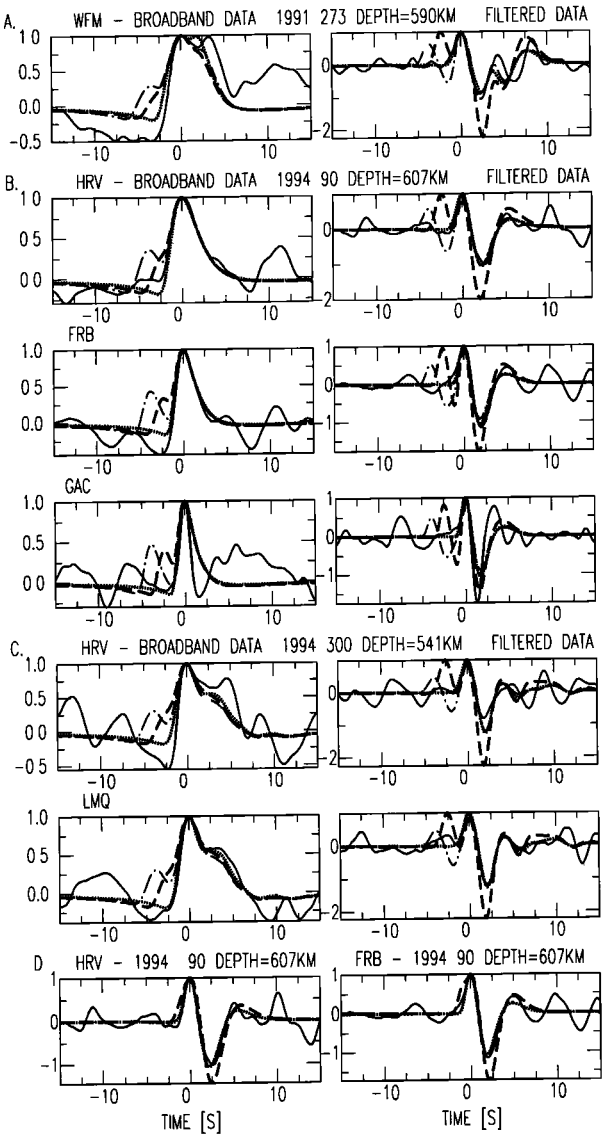

Figure 3. Comparison of observed and synthetic seismograms: a-c - broad-band (left) and high-pass filtered (right) displacement records of SKS phase (solid line). Synthetic seismograms are for IASP91 (dotted line), and models containing 20 and 30 km thick ULVZ (dashed and dot-dashed line, respectively); d - high-pass filtered displacement records of SKS phase (solid line) and synthetic seismograms for IASP91 (dotted line) and model with 10 km thick ULVZ (dashed line). Event date and station are shown on each plot.

ment. Figure 3 shows the radial (R) component of some of the deconvolved seismograms with a simple and short source time function. These seismograms are compared with the corresponding synthetic seismograms. The maximum amplitudes of both are normalized to unity. The synthetics are calculated for IASP91 and model with ULVZ at the source side. In agreement with Garnero et al. (1998), the S and P-wave velocities in ULVZ are reduced relative to IASP91 by 30% and 10%, respectively, and the assumed thickness of the layer is 30, 20 or 10 km. The differences between the synthetics and the real seismograms are not well seen in the broad band,

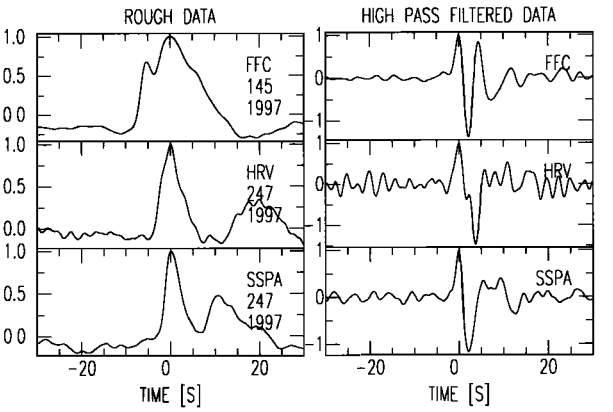

Figure 4. Broad-band (left) and high-pass filtered (right) records corresponding to common conversion point. Station and event are written on each plot.

and to make them more clear, the broad-band records were high-pass filtered with a cut-off at 0.2 Hz.

On the filtered records, one can see that the observed SKS consists of a sharp main lobe, which is followed by weaker oscillations. Contrary to the real records, the synthetic seismograms for ULVZ with a thickness of 30 km contain a precursor, which is only twice weaker than the main signal. The synthetics for a 20 km thick layer contain two main lobes of similar amplitudes, which are followed by the downward motion, about twice stronger than in the real data. The two lobes correspond to S^SKS and S^PKS phases in Figure 2. The amplitude ratio between S^PKS and S^SKS phases is much larger than the ratio between their transmission coefficients, because the tail of S^PKS interferes destructively with S^SKS phase. For ULVZ 10 km thick the discrepancy is less striking, but the main lobe in the synthetics is broader than in the real data. The synthetics for IASP91 provide much better fit to the real data than those for the models with the reduced S wave velocity.

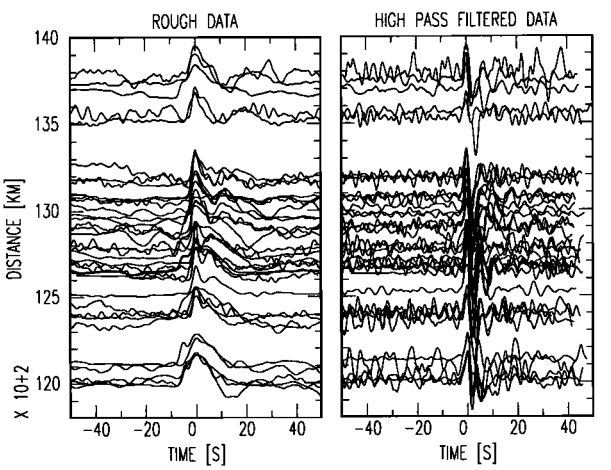

Figure 5. Broad-band (left) and high-pass filtered (right) records corresponding to Table 1. The traces with inverse polarity are multiplied by -1, amplitudes are normalized to unity, and the main lobes are aligned.

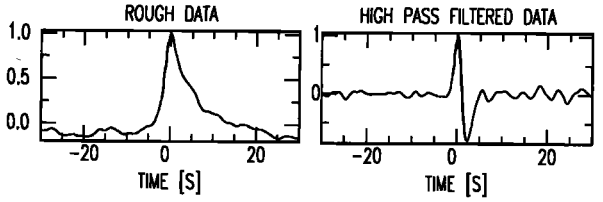

Figure 6. Stacks of most broad-band (left) and high-pass filtered (right) records displayed in Figure 5. The explanation and list of rejected data are in the text.

Among seismograms listed in Table 1, all seismograms of event 94/03/09 were found too complicated, apparently owing to a complicated source process. Two seismograms of event 97/05/25 (FFC and CCM) in the broad band contain something which looks like a precursor. One of these seismograms is shown in Figure 4, where it is compared with two other seismograms which have practically the same conversion point. After high-pass filtering the suspected precursor becomes stronger than the main phase, whereas the other seismograms contain no visible precursor at all. These data suggest that the suspected precursor can not be interpreted as the phase converted in the D" layer. A similar conclusion is made with respect to the other anomalous seismogram. In other filtered records, the waveforms are fairly similar irrespectively of the actual source function, and to enhance signal/noise ratio we have stacked them. Prior to stacking, the first maxima of the seismograms were aligned, the traces with inverse polarity were multiplied by -1 and the traces were normalized to unity (Figure 5). Fluctuation of the upper boundary of the ULVZ in the range of several kilometers would produce a neglegible effect on the amplitude of the precursor in the filtered stack. In the stack (Figure 6), no precursor with an amplitude larger than about 5% of the amplitude of the main signal is seen within several seconds preceding the first motion. Since the transmission coefficient for S^PKS is roughly proportional to the S-wave velocity contrast at the discontinuity, this implies that the S-wave velocity contrast at the top of the ULVZ is much less than about 10%. On the assumption of partial melting, the required P-wave velocity contrast would be less than about 3%, which is inconsistent with the values of the ultra-low P-wave velocity reported elsewhere.

Conclusion

Our analysis demonstrates that the S velocity drop predicted by the hypothesis of melting does not exist in the sampled area, if the thickness of the layer is around 10-15 km or more. This implies that either ULVZ is not related to melting, or the layer is too thin to be resolved with our technique. A possibility of melting in a thicker zone still exists, if melt is in many very thin layers. In the resulting fine-layered medium the horizontal P-wave velocity can be low, but the S-wave velocities are strongly different from those predicted for ULVZ [Vinnik et al. 1998]. Significant anisotropy (transverse isotropy) rather than the ultra-low S-wave velocity is diagnostic for this medium.

Acknowledgments. This is an I.P.G.P contribution 1665, UMR CNRS 7580. Comments from V. Farra, R. Kind, J. Castle and H. Paulssen are appreciated. A partial support of this research by INTAS-RFBR 95-0865 is acknowledged.

References

Choy, G.L. Theoretical seismograms of core phases calculated by frequency-dependent full wave theory, and their interpretation, *Geophys. J. R. Astron. Soc.*, *51*, 275–312, 1977.

Choy, G.L., & V.F. Cormier, Direct measurement of the mantle attenuation operator from broad band P and S waveform, *J. Geophys. Res.*, *91*, 7326–7342, 1986.

Doornbos, D.J., & T. Hilton, Models of the core-mantle boundary and the travel times of internally reflected core phases, *J. Geophys. Res.*, *94*, 15,741–15,751, 1989.

Garnero, E.J., S.P. Grand, & D.V. Helmberger, Low P wave velocity at the base of the mantle, *Geophys. Res. Lett.*, *20*, 1843–1846, 1993.

Garnero, E.J., & V.D. Helmberger, Seismic detection of a thin laterally varying boundary layer at the base of the mantle beneath the central Pacific, *Geophys. Res. Lett.*, *23*, 977–980, 1996.

Garnero, E.J., & V.D. Helmberger, Further structural constraints and uncertainties of a thin laterally varying ultralow-velocity layer at the base of the mantle, *J. Geophys. Res.*, *103*(6), 12,495–12,509, 1998.

Garnero, E. J., J. Revenaugh, Q. Williams, T. Lay, & L.H. Kellogg, Ultralow velocity zone at the core-mantle boundary, *The core-mantle boundary region. Geodynamic series*, *28*, 319–334. M. Gurnis, M. E. Wysession, E. Knittle, B. A. Buffett *editors*, 1998.

Kennett, B.L. (ed), *IASPEI 1991, Seismological tables.* Australian National University, 1991.

Kind, R. & G. Mueller, Computations of SV waves in realistic Earth models, *J. Geophys.*, *41*, 142–162, 1975.

Ruff, L.J. & A.D. Miller, Rupture process of large earthquakes in the northern Mexico subduction zone, *PAGEOPH*, *142*, 101–172, 1994.

Vinnik, L., L. Breger, & B. Romanowicz, Anisotropic structures at the base of the Earth's mantle, *Nature*, *393*, 564–567, 1998.

Weber, M., Computation of body wave seismograms in absorbing 2-D media using gaussian beam method: comparison with exact methods, *Geophys. J.*, *92*, 9–24, 1988.

Williams, Q., & E.J. Garnero, Seismic evidence for partial melt at the base of Earth's mantle, *Science*, *273*, 1528–1530, 1996.

(Received August 9, 1999; revised October 28, 1999; accepted March 6, 2000.)